Dynamic intralaminar fracture toughness characterisation of unidirectional carbon fibre-reinforced polymer composites using a high-speed servo-hydraulic test set-up

Sanghyun Yoo[1*], Denis Dalli[2,3], Giuseppe Catalanotti[2,4], Nathalie Toso[1], Fiona Kessel[1], Heinz Voggenreiter[1]

[1] Institute of Structures and Design, German Aerospace Center (DLR), Stuttgart, Germany
[2]Advanced Composites Research Group (ACRG), School of Mechanical and Aerospace Engineering, Queen's University Belfast, Ashby Building, Stranmillis Road, Belfast, UK
[3]DEMec, Faculdade de Engenharia, Universidade do Porto, Rua Dr.Roberto Frias, s/n, 4200-465, Porto, Portugal
[4]Escola de Ciências e Tecnologia, Universidade de Évora, Colégio Luis António Verney, Rua Romão Ramalho, 59, 7000-671 Évora, Portugal

Abstract

This paper presents an experimental investigation on the intralaminar fibre-dominated fracture of unidirectional (UD) IM7/8552 carbon-epoxy composites, loaded under quasi-static (QS) and intermediate strain rates (IR). Dynamic tensile testing is carried out using a previously proposed test methodology involving a high-speed servo-hydraulic test machine, equipped with a slack adapter, and Digital Image Correlation (DIC), with the aim of providing an alternative means to Split-Hopkinson pressure bar testing for the characterisation of similar composite materials at intermediate-to-high strain rates. Three sizes of Double-Edge Notched Tension (DENT) specimens are tested at QS and IR to obtain the mode I intralaminar fracture toughness. The results of the fracture toughness tests compare well with literature data, supporting the proposed methodology. This study is a first step towards standardising a more easily accessible test method for characterising the mechanical properties of fibre-reinforced polymer (FRP) composites over a broad range of dynamic strain rates.

Keywords: Strain-rate testing; Carbon fibre composites; Digital Image Correlation; Fracture toughness; Size effect.

*Corresponding author: Sanghyun Yoo

Email: Sanghyun.Yoo@dlr.de

Tel: +49-711-6862-573

1 Introduction

The experimental determination of the fracture toughness of fibre-reinforced polymer (FRP) composites is an essential precursor to performing complex numerical simulations that make use of continuum damage [1-3] or finite fracture mechanics material models [4, 5], whereby material softening parameters are derived from the crack resistance curve (*R*-curve) [6-8]. The accuracy of such simulations is strongly dependent on the quality of experimentally-derived input material parameters, and as a result of the lack of standardised intermediate and high strain rate characterisation methods, it is still tough to obtain accurate numerical predictions for the behaviour of dynamically loaded composite structures. Hence, there is a continued reliance on experimental validation for said structures [9].

Fracture toughness of composites is generally categorised into 'interlaminar' and 'intralaminar', distinguishing between crack growth in between plies and that within individual plies, respectively. Measurement of the mode I interlaminar fracture toughness using the Double Cantilever Beam (DCB) specimen under quasi-static loading has been extensively documented in the last decades and has even been standardised in ASTM 5528 [10] and ISO 15024 [11]. Similarly, the quasi-static experimental determination of mode II and mixed-mode I-II interlaminar fracture toughness properties have also been standardised [12, 13]. Conversely, intralaminar fracture toughness tests have not yet reached a consensus for standardisation, not even for the most straightforward quasi-static loading cases in mode I and compression. Although there has been significant effort placed on developing stable crack propagation techniques, such as Compact Tension (CT) and Compact Compression (CC), the test methodologies and data reduction techniques for the latter still suffer from user-dependent subjectivity (crack length incremental measurement), which affects the final estimate of the fracture toughness parameters [14]. More recent work focusing on unstable crack propagation methods allows for more objectivity in the determination of these same parameters [15, 16], and is based on the size effect method proposed by Bažant [17]. This unstable crack propagation technique was first applied by Catalanotti et al. [18] for measuring the mode I and compression quasi-static intralaminar fracture toughness of unidirectional (UD) composites, using double-edge notched tension/compression (DENT/C) specimens.

The experimental challenge in measuring fracture toughness is further exacerbated when testing at higher loading rates, as most stable crack propagation coupon geometries such as DCB and CT suffer from asymmetrical load introduction, which leads to the crack being propagated under mixed-mode conditions [9]. The effect of strain rate on interlaminar fracture toughness has already been well investigated and documented in review papers [9, 19, 20]. However, no consensus has been reached on the actual strain rate dependence of these interlaminar properties, and furthermore, none of the experimental methods have been agreed upon for standardisation, even though the issue of asymmetrical load introduction has been overcome [21-23].

There is a similar disagreement on the effect of strain rate on intralaminar fracture toughness, as none of the presently available literature is able to back up its quantitative results with a factual explanation of the changing fracture phenomena from quasi-static to dynamic regimes, and this argument is compounded by a significantly lower volume of research data available on the dynamic characterisation of intralaminar fracture toughness. The current state of the art in dynamic intralaminar fracture toughness testing is that proposed by Kuhn et al. [24-26], whereby the size effect method was adapted and used in combination with a Split-Hopkinson Pressure Bar (SHPB) set-up. Although this equipment is very suitable for high strain rate testing, it also requires unique technical expertise for data reduction and is not a typical test equipment found in most material characterisation laboratories. Furthermore, its applicability in the intermediate strain rate range is quite limited. Thus, literature has shown there is an active need to provide more research data in the field of dynamic intralaminar fracture toughness characterisation, as well as finding more accessible test equipment and methods with which said characterisation could be performed reliably and accurately.

This work seeks to address both issues by experimentally assessing the possible applicability of a more easily-accessible high-speed servo-hydraulic testing machine, coupled with a previously developed slack adapter that handles inertial effects [27-29], which also offers a broader test range of intermediate-to-high strain rates than standard SHPB set-ups.

2 Materials and methodology

2.1 Materials

Test specimens were manufactured out of Hexply® IM7-8552, a unidirectional carbon-epoxy composite. Square 300 mm panels were first prepared in balanced cross-ply lay-ups of $[0°/90°]_{3s}$ and $[0°/90°]_{4s}$ to achieve nominal thicknesses of 1.5 and 2 mm, for intralaminar fracture toughness and in-plane test coupons, respectively. Each panel was cured under vacuum, in an autoclave in accordance with the manufacturer's recommendations, at 180 °C and 6 bar atmospheric pressure [30]. Selected panels were subjected to ultrasonic (US) scanning using an Olympus OmniScan MX2 to ensure their post-manufacturing quality. Finally, the desired specimen geometries were machined out using CNC milling. The notches of the DENT specimens had a tip diameter of 1.5 mm, which is slightly higher than the 1 mm value typically found in literature, and was a result of a limitation of the available minimum milling bit size.

For dynamic testing, the specimens were adhesively bonded with slotted grips, thereby reducing the overall weight of the assembly compared to conventional clamping mechanisms. These grips also have threaded endcaps that allow for a rapid connection to the slack adapter of the high-speed testing machine. Since this grip weight directly influences the magnitude of the inertial effect, the proposed lightweight clamping mechanism, especially on the heavier lower end that includes the sliding bar, increases the natural frequency of the test system to help minimise the oscillation in load signals. The clamping technique using adhesive bonding was adapted from the technique used for similar SHPB testing [31-33], using a two-component epoxy (Scotch Weld DP490, 3M™). The bonds were post-cured in a furnace at 65 °C for 2 hours to improve their strength, according to the manufacturer's recommendations. The procedure to prepare the specimens with the adhesive clamping is shown in Fig. 1 (b).

2.1.1 Specimens for in-plane elastic testing

Standard tension specimens were tested in accordance with ASTM 3039/D3039M-17 [34] to find the elastic properties of the cross-ply laminate (elastic modulus and Poisson's ratio). Furthermore, ± 45° tensile specimens were cut from the same cross-ply laminates and tested quasi-statically in accordance

with ASTM standard 3518/D3518-18 [35], thus determining the in-plane elastic shear properties. In this case, it was necessary to also acquire these properties under dynamic loading, as the matrix-dominated shear elasticity is definitely strain-rate dependent.

Fig. 1 (a) shows an image of three different specimen geometries, namely QS-ASTM, QS-w16, and QS-w08, for in-plane shear testing, with specimen sizes summarised in Table 1. The smaller analogous rectangular geometry, QS-w08, with a downscaled gauge area having a maintained length-to-width proportion of 2.5, was chosen for dynamic testing (refer to Fig. 1 (b)). Minimum three tests were conducted quasi-statically for each specimen geometry (refer to Table 1), and three tests were carried out for the QS-w08 geometry at intermediate strain rates.

It was necessary to use small specimens to measure in-plane shear properties in dynamic testing in order to minimise undesired oscillations in force measurement and achieve homogeneous deformations within the gauge section. In the field of dynamic testing at intermediate strain rates, no standard currently exists for FRP composites, and standards from quasi-static test regimes are not directly applicable due to the required changes and adaptations in the experimental set-up and specimen geometry. These modifications make it difficult to correlate the quasi-static and dynamic shear behaviours observed for FRPs. The initial comparative study conducted for quasi-static testing aimed to better understand the influence of specimen geometry on the in-plane shear behaviour, thus enabling correlation of the obtained data to that acquired later from dynamic testing.

2.1.2 Specimens for intralaminar fracture toughness testing

In order to use the size effect law to calculate the mode I intralaminar -curve, geometrically scaled DENT specimens of three different sizes were manufactured, as shown in Fig. 2. These specimens were tested under both quasi-static and dynamic loading regimes in order to create a baseline comparison for the fracture toughness properties as was done previously in the literature [25]. Six specimens were tested for each size and strain rate.

2.2 Test methods

2.2.1 Slack adapter for the servo-hydraulic machine

High-speed servo-hydraulic machines are the typical first choice for obtaining dynamic material properties at intermediate strain rates due to their unique capability of applying large displacements at high speeds of up to 20 m/s. To apply a constant speed during the test, a clamping mechanism is commonly used to engage with the specimen once the target speed has been reached.

In this work, a slack adapter was used as the clamping mechanism, consisting of a sliding bar which enters into contact (directly or through an interposed damping element) with a slack sleeve once the desired speed of the actuator has been reached. The contact between bar and sleeve may cause a substantial shock impulse that could lead to system ringing in the experimental set-up [6,9] and this could consequently hinder the determination of the true mechanical properties of the material because it influences the quality of load signals [36]. Fig. 3 shows the recently developed slack adapter that minimises the undesired inertial effect and produce high-quality results by having a higher natural frequency, the virtue of its reduced weight. The applicability of the developed slack adapter to a variety of test materials has already been reported in the literature [27-29].

2.2.2 Quasi-static testing

Fig. 4 (a) and (b) show the two experimental set-ups for the quasi-static testing of the ± 45° tensile specimens and DENT specimens, respectively. The longitudinal and ± 45° tensile specimens were tested using a Zwick/Roell 1484 universal testing machine (UTM) equipped with a 200 kN load cell, and standard hydraulic grips applying a clamping pressure of 20 MPa. Loading was applied under displacement control at a rate of 2 mm/min up to failure. A 3D-Digital Image Correlation (DIC) stereo system (Q-400, LIMESS Messtechnik u. Software GmbH, Germany) was used to obtain the strain fields with a spatial resolution of approximately 13 μm/pixel. Acquired images were post-processed with INSTRA 4D software from Dantec Dynamics. A stochastic speckle pattern was sprayed on each specimen using an airbrush, where the average black particle size was approximately 40 μm. The frame rate and resolution were adjusted depending on specimen size, as the test duration was shorter for smaller

specimens (refer to Table 2). The DENT fracture toughness specimens were tested in a Zwick/Roell Z100 UTM equipped with a 100 kN load cell at a constant displacement rate of 1mm/min.

2.2.3 Intermediate strain-rate testing

An identical dynamic test set-up was used for both the ± 45° tensile and DENT specimens, as shown in Fig. 4 (c). The ± 45° tensile tests were performed at five nominal strain rates ranging from 0.1 to 300 s^{-1} (0.1, 10, 100, 200 and 300 s^{-1}). An Instron® VHS 100/20 high-speed servo-hydraulic test machine was used with a piezo-electric load cell with a capacity of ± 120 kN (Kistler-9317B, Kistler Instrumente GmbH, Germany). The force signals were amplified with a Kistler type 5011B charge amplifier. DIC images were captured using a high-speed camera (FASTCAM SA-Z, Photron , Japan) with adjusted frame rates and resolutions to obtain sufficient images during the testing at different strain rates (refer to Table 2). Those images were post-processed with GOM Correlate. The strain field was calculated using a facet size of 15 pixels and a facet step of 5 pixels. For in-plane shear testing, an average strain value over the nominal gauge area between grip edges is used to calculate longitudinal and transverse strain, and the average of an initial notch area with the length of 10 mm strain field is used to deduce axial strain of DENT specimens.

In addition, the high-speed images were synchronised with the force signals through NI-DAQ (USB-6251 BNC, National Instruments™, USA). A damping material made of soft acrylic tape (3M™ 5952 VHB) was placed on the contact surface between the cone and the sleeve so that the hard metal-to-metal contact could be softened. Each strip of tape was 12 mm ×15 mm × 1 mm (length × width × thickness) and was replaced for each specimen to ensure each test was carried out with an equally uncompacted damper. A total of six strips of tapes were evenly attached to the conical contact surface, leading to a damped contact surface of 1080 mm , corresponding to 55 % of the full contact surface between the cone and the sleeve. The dynamic stress-strain responses presented later in this paper are raw data since the use of digital filtering may eliminate some of the important information [37, 38].

2.2.4 Fractography

The fractured surfaces of samples tested at different strain rates were analysed using a scanning electron microscope (SEM, Gemini ultra plus from Zeiss Group). An AsB detector (Angle selective Backscatter) and 10 kV electron high tension (ETH) voltage were used for the imaging.

2.3 The size effect method

An analytical model to calculate the intralaminar fracture toughness and the associated *R*-curve was initially tested by Catalanotti et al. [39] based on Bažant's size effect method for quasi-brittle materials [17]. This paper presents an outline of this method, and the reader is referred to the literature [15, 25, 39] for more detailed descriptions of its derivation.

For unstable mode I crack propagation, the critical driving force curves, G_I, for different specimen sizes at their respective peak loads, P_u, are tangential to the *R*-curve, R, at distinct points as shown in Fig. 5. Hence, the *R*-curve can be derived as an envelope of the critical driving force curves of geometrically-scaled specimens, and this relationship can be defined as:

$$\begin{cases} G_I(\Delta a) = R(\Delta a) \\ \frac{\partial G_I(\Delta a)}{\partial \Delta a} = \frac{\partial R(\Delta a)}{\partial \Delta a} \end{cases} \quad (1)$$

where Δa is crack extension. The size effect law can be experimentally determined by testing geometrically similar specimens and then fitting a bilogarithmic regression through the measured peak nominal stresses. When the size effect law, $\sigma_u = \sigma_u(w)$ is known, the *R*-curve can be written again as:

$$R(\Delta a) = \frac{1}{\acute{E}} w \sigma_u^2 k^2 \left(\alpha_0 + {\Delta a}/{w}\right) \quad (2)$$

where $\acute{E}$ is the equivalent modulus, w is the chosen characteristic size (in this case equivalent to half the total specimen width), σ_u is the peak nominal stress ($\sigma_u = {P_u}/{(2wt)}$, where t is the specimen thickness), α_0 is the initial value of the shape parameter ($\alpha_0 = {a_0}/{w}$), and k is the correction factor for geometry and orthotropy. This factor was numerically estimated using the Virtual Crack Closure Technique (VCCT) in a Finite Element (FE) software package.

The equivalent modulus, $\acute{E}$ was calculated from the following equation:

$$\acute{E} = \lambda^{1/4}\sqrt{E_{11}E_{22}\left(\frac{2}{1+\rho}\right)} \quad (3)$$

where, $E_{11}$and E_{22} are the elastic moduli in the directions parallel and perpendicular to the crack (for a balanced cross-ply laminate), while λ and ρ are dimensionless orthotropic elastic parameters defined as:

$$\lambda = \frac{E_{22}}{E_{11}},\ \rho = \frac{\sqrt{E_{11}E_{22}}}{2G_{12}} - \sqrt{\nu 12\,\nu 21} \quad (4)$$

where $\nu_{12}$and ν_{21} are the major and minor in-plane Poisson's ratios.

By keeping the specimen shape parameters fixed and differentiating Eq. (2), while remembering that the *R*-curve is a material parameter independent of specimen width ($\partial R/\partial w = 0$):

$$\frac{\partial}{\partial w}\left(w\sigma_u^2 k^2\right) = 0 \quad (5)$$

Solving Eq. (5) for $w = w(\Delta a)$, and substituting w back into Eq. (2), the $R(\Delta a)$ curve is obtained.

3 Results and Discussion

3.1 Elastic property characterisation

3.1.1 Quasi-static tensile testing

The quasi-static tension properties for the balanced cross-ply laminates are reported in Table 3, including the elastic modulus for the two-principal fibre-dominated directions of 85.31 ± 2.99 GPa, and the major in-plane Poisson's ratio of 0.029 ± 0.003. No dynamic testing was conducted for characterisation at higher strain rates, as the longitudinal fibre-dominated elastic mechanical properties are known to be strain-rate independent for unidirectional carbon composites [40, 41].

3.1.2 Quasi-static in-plane shear testing and specimen geometry effects

Fig. 6 shows shear stress-strain data from the three different specimen geometries tested quasi-statically. The average shear modulus of the QS-ASTM specimens is 3.4 % higher than that of the QS-w08

specimens, a difference that falls within the standard deviation of the averaged data, hence indicating no meaningful difference. The QS-w08 specimens presented an increase of approximately 9 % in shear strength. The ASTM standard defines this failure strength as the stress corresponding to 5 % strain, as above strain level the ± 45° tensile specimen exhibits significant fibre scissoring, with the fibres realigning towards the tensile direction, and the composite thus experiences a significant level of tensile stress in addition to shear. Thus, the fibre rotation will result in an overestimated shear strength if failure is assumed to occur at strain values higher than 5 % [42, 43]. The tested specimens show a chevron type failure which can be observed post-mortem in Fig. 7.

The reduction in gauge section size was thus shown to have an almost negligible effect on the overall shear behaviour, except for the failure strain. However, the latter is highly dependent on the stress state of the rotated fibres, and the degree of which varies depending on the gauge section size. This indicates the suitability of the smaller specimen size for use in intermediate strain rate testing, and enables the correlation of quasi-static and dynamic in-plane shear data.

3.1.3 Intermediate strain rate shear testing

Fig. 8 presents raw signals of force-time data, with superimposed displacement profiles, from the dynamic in-plane shear tests conducted at three different strain rates (a-c), together with the derived stress-strain data (d). No significant oscillations were observed in the raw force signals up to the point of fracture, indicating that these signals were suitable without the need of any filtering.

Fig. 9 shows a comparison of the in-plane shear stress-strain data obtained from QS-w08 specimens for quasi-static and dynamic strain rates up to 300 s^{-1}. Significant strain-rate effects were observed for the shear modulus, failure strength, and overall plasticity behaviour. At 300 s^{-1}, the shear modulus increased by 21.7 %, while shear strength rose by 59.6 %, when compared with their quasi-static values. The increase of shear strength and modulus are in good agreement with reported results in the literature [44-47] for in-plane shear properties measured with ± 45° tensile tests. Similar observations can be found in the literature for other off-axis tensile test campaigns [31, 48-51].

On the other hand, Fig. 9 clearly shows a decrease in failure strain at higher strain rates as reported for this same fibre-resin system in literature [50]. Furthermore, Cui et al. [44] reported that the final failure strain of $\pm 45°$ carbon-epoxy laminates is reduced with increasing strain rates after taking into account the effect of fibre rotation. The measured in-plane shear properties of IM7/8552 are summarised in Table 2. Fig. 10 presents a logarithmic strain-rate based comparison of the in-plane shear strength variation for a number of composite materials available in the literature [31, 41, 44-48, 50-56], together with values obtained in this study, each normalised with respect to their quasi-static values. This comparative study shows that the results obtained using the newly developed test device are quite similar to what is reported in the literature (including results obtained from SHPB tests), increasing confidence in the capability of this experimental set-up to acquire reliable dynamic material parameters for FRP composites tested at intermediate strain rates.

3.2 Intralaminar fracture toughness

3.2.1 Intralaminar fracture toughness and crack resistance curve

Table 3 reports the input elastic material data used in the VCCT model as part of the data reduction to calculate the intralaminar *R*-curve.

Fig. 11 presents the dynamic nominal stress-strain data for the DENT specimens tested at strain rates of 60 and 100 s^{-1}. The results evidence a linear increase in stress up to the point of sudden failure, indicating that there was no evident plasticity effect occurring before peak load, ensuring that the linear-elastic assumptions taken in the VCCT model are actually valid.

Table 4 summarises the average peak nominal stresses for all the quasi-static and dynamic DENT specimens, with Fig. 12 presenting this same data in order to visually highlight the evident size effect, as well as the increase in peak stress at higher strain rates. This same size effect is also highlighted in Fig. 13, which presents the bilogarithmic regression fits of the experimental peak nominal stress data for all three tested strain rates (a-c), including their 95 % confidence intervals, as well as a comparison of the average fits (d). The slight increase in peak nominal stresses from quasi-static to 60 s^{-1} was also reported in the literature for the same material system tested using the SHPB set-up [25]. There was no

significant change in σ_u between the 60 and 100 s^{-1} tests. In summary, all three regressions fall within the 95 % confidence interval of the QS tests, indicating that the change in peak nominal stresses from QS to intermediate strain rates is not statistically significant. The bilogarithmic fitting coefficients (M,N) are summarised in Table 5. The R-curve for each set of specimens was derived using these fitting coefficients, together with the previously calculated equivalent moduli ($\acute{E}$) and the correction factors obtained from VCCT. The steady-state fracture toughness (R_{ss}) and associated critical crack extension (c_f) values are also summarised in Table 5 for all tested strain rates. These R-curves, with their 95 % confidence intervals (derived from their corresponding size effect regression intervals) and critical driving force curves, as well as an overall comparison, are presented in Fig. 14. It is important to note that these are R-curves for the balanced cross-ply laminates and that by assuming the 90^0 plies to have a negligible contribution to the overall fracture toughness, the R-curves for the 0^0 plies would be double in magnitude [39].

When combining the variations in elastic properties noted for the various strain rates (Table 3) together with the slight variations in the bilogarithmic fits of Fig. 13, the derived R-curves of Fig. 14 for dynamic testing do not fall within the 95 % confidence limit of the QS curve, unlike what was observed for the bilogarithmic regressions when considered in isolation. However, it can be noted that there is still no significant difference between the specimens tested at 60 and 100 s^{-1}, even for their R-curves, as the mean values easily fall within the confidence intervals of each other. It is thus quite difficult to definitively confirm the existence of a strain rate dependency of the mode I intralaminar fracture toughness of UD IM7/8552 composites. More experiments need to be performed in order to acquire a more definitive answer on the real strain rate dependency of this parameter, and this can only be achieved by modifying the experimental set-up to enable the testing of larger specimen widths, thus increasing the confidence in the bilogarithmic size effect regressions. This limiting factor on specimen size is a drawback that has similarly hampered results obtained using the SHPB set-up [15].

3.2.2 Fractographic analysis

The fracture surfaces of the DENT specimens were examined via scanning electron microscopy (SEM) to identify distinct damage mechanisms that characterise the fracture process zone at quasi-static and

dynamic loading conditions (Fig. 15): namely, delamination at the 0°/90° interface (Fig. 15 (a-1), and (a-2)); fibre fracture and pull-out (Fig. 15 (b-1), (b-2), and (b-3)); and matrix fracture and fibre/matrix debonding (Fig. 15 (c-1), (c-2) and (c-3)). The synergetic effect of these different damage mechanisms may vary from quasi-static to dynamic strain rates and could contribute to the variation in the measured intralaminar fracture toughness. However, since SEM images can only provide a qualitative assessment of failure modes, this alone is not sufficient to deduce any quantitative explanations for the change in intralaminar fracture toughness with strain rate.

3.2.3 Comparison with literature

Table 6. compares the quasi-static steady-state energy release rate for mode I intralaminar fracture of the 0^0 ply for UD IM7/8552 composites, measured from the current study with previously reported values from the literature [25, 39, 57-63]. From all the available literature, only the OCT specimens tested by Li et al. [61] managed to exceed the G_{IC} values measured in this work. A large scatter can be observed within the reported values, and it is difficult to identify an actual consensus value for G_{IC}. This scatter can result from multiple factors: (a) the testing conditions, (b) storage, lay-up and consolidation methods, (c) specimen manufacturing, and (d) tested specimen geometry. One other factor which might have contributed to the seemingly high value of G_{IC} in the present work is the notch tip diameter of 1.5 mm, which is larger than that of used for the specimens tested in the literature of Table 6, where the typical value ranged from 0.15 mm to 1 mm. Only Kuhn et al. [25] tested DENT specimens with the same notch tip diameter as the present study, and their value of G_{IC} was also on the high side compared to most other literature data. Although it has been reported that the peak load of DENT specimens subjected to unstable crack propagation is not sensitive to the notch tip size, this has only been proven for 2D woven composites [15]. The difference of 31 % between the values of Kuhn et al. [25] and those presented here are more probably a result of the different consolidation methods, where this study favoured the manufacturer's guidelines of using an autoclave over a hot-press. This change could have resulted in different fibre volume fractions in the laminates, leading to a different performance under mode I loading, in a similar manner to what was already observed in literature [64].

At a strain rate of 60 s^{-1}, the normalised value of mode I intralaminar fracture toughness was 24 % higher than that of quasi-static tests, while that of Kuhn et al. [25] increased by 19 %, as shown in Fig. 16. This similar increase in magnitude suggests that the intralaminar G_{IC} of the tested material does in fact experience a strain-rate dependency. However, any solid conclusions on the matter will necessitate further testing, as already discussed.

4 Conclusion

This paper detailed and discussed the measurement of both quasi-static and dynamic material properties at intermediate strain rates, the latter of which was performed using a recently developed experimental set-up using a high-speed servo-hydraulic machine equipped with a slack adapter. The tests were able to successfully characterise the in-plane shear behaviour and mode I intralaminar fracture toughness of a UD carbon-epoxy composite. For intralaminar fracture toughness, geometrically scaled DENT specimens were tested in combination with the size effect methodology in order to obtain the *R*-curve of the cross-ply laminate, and that of the 0° ply.

The recently developed test method based on the high-speed servo-hydraulic test machine has been successfully applied to measure the in-plane shear behaviour and intralaminar fracture toughness of FRP composites. This provides engineers with a more viable experimental option for acquiring fracture toughness properties at intermediate strain rates, apart from the well-established SHPB set-up. Furthermore, this test set up extends the possibilities of characterising the material over a larger range of strain rates by covering the intermediate range between quasi-static and high strain rate, unlike the standard SHPB set-up which can only be used at the higher end of the strain rate range.

Acknowledgements

The authors gratefully acknowledge the financial support of the project ICONIC — Improving the Crashworthiness of Composite Transportation Structures. ICONIC has received funding from the European Union's Horizon 2020 research and innovation programme under the Marie Skłodowska-

Curie grant agreement No 721256. The content reflects only the authors' views, and the agency is not responsible for any use that may be made of the information it contains.

Data availability

The raw/processed data required to reproduce these findings cannot be shared at this time as the data also forms part of an ongoing study.

5 References

[1] Falzon BG, Apruzzese P. Numerical analysis of intralaminar failure mechanisms in composite structures. Part I: FE implementation. Composite Structures. 2011;93:1039-46.
[2] Falzon BG, Apruzzese P. Numerical analysis of intralaminar failure mechanisms in composite structures. Part II: Applications. Composite Structures. 2011;93:1047-53.
[3] Williams KV, Vaziri R, Poursartip A. A physically based continuum damage mechanics model for thin laminated composite structures. International Journal of Solids and Structures. 2003;40:2267-300.
[4] Andersons J, Tarasovs S, Spārniņš E. Finite fracture mechanics analysis of crack onset at a stress concentration in a UD glass/epoxy composite in off-axis tension. Composites Science and Technology. 2010;70:1380-5.
[5] Reinoso J, Arteiro A, Paggi M, Camanho PP. Strength prediction of notched thin ply laminates using finite fracture mechanics and the phase field approach. Composites Science and Technology. 2017;150:205-16.
[6] Dávila CG, Rose CA, Camanho PP. A procedure for superposing linear cohesive laws to represent multiple damage mechanisms in the fracture of composites. International Journal of Fracture. 2009;158:211-23.
[7] Maimí P, Camanho PP, Mayugo JA, Dávila CG. A continuum damage model for composite laminates: Part I – Constitutive model. Mechanics of Materials. 2007;39:897-908.
[8] Maimí P, Camanho PP, Mayugo JA, Dávila CG. A continuum damage model for composite laminates: Part II – Computational implementation and validation. Mechanics of Materials. 2007;39:909-19.
[9] May M. Measuring the rate-dependent mode I fracture toughness of composites – A review. Composites Part A: Applied Science and Manufacturing. 2016;81:1-12.
[10] ASTM D5528-13, Standard Test Method for Mode I Interlaminar Fracture Toughness of Unidirectional Fiber-Reinforced Polymer Matrix Composites. West Conshohocken, PA: ASTM International; 2013.
[11] ISO 15024:2001, Fibre-reinforced plastic composites — Determination of mode I interlaminar fracture toughness, GIC, for unidirectionally reinforced materials. Geneva, Switzerland: International Organization for Standardization; 2001.
[12] ASTM D7905/D7905M-19e1, Standard Test Method for Determination of the Mode II Interlaminar Fracture Toughness of Unidirectional Fiber-Reinforced Polymer Matrix Composites. West Conshohocken, PA, : ASTM International; 2019.
[13] ASTM D6671/D6671M-19, Standard Test Method for Mixed Mode I-Mode II Interlaminar Fracture Toughness of Unidirectional Fiber Reinforced Polymer Matrix Composites. West Conshohocken, PA, : ASTM International; 2019.
[14] Laffan MJ, Pinho ST, Robinson P, McMillan AJ. Translaminar fracture toughness testing of composites: A review. Polymer Testing. 2012;31:481-9.

[15] Dalli D, Catalanotti G, Varandas LF, Falzon BG, Foster S. Mode I intralaminar fracture toughness of 2D woven carbon fibre reinforced composites: A comparison of stable and unstable crack propagation techniques. Engineering Fracture Mechanics. 2019;214:427-48.
[16] Dalli D, Catalanotti G, Varandas LF, Falzon BG, Foster S. Compressive intralaminar fracture toughness and residual strength of 2D woven carbon fibre reinforced composites: New developments on using the size effect method. Theoretical and Applied Fracture Mechanics. 2020;106:102487.
[17] Bažant ZP, Planas J. Fracture and Size Effect in Concrete and Other Quasibrittle Materials. London: CRC Press, 1998.
[18] Catalanotti G, Xavier J, Camanho PP. Measurement of the compressive crack resistance curve of composites using the size effect law. Composites Part A: Applied Science and Manufacturing. 2014;56:300-7.
[19] Jacob GC, Starbuck JM, Fellers JF, Simunovic S, Boeman RG. The effect of loading rate on the fracture toughness of fiber reinforced polymer composites. Journal of Applied Polymer Science. 2005;96:899-904.
[20] Siddique A, Abid S, Shafiq F, Nawab Y, Wang H, Shi B, et al. Mode I fracture toughness of fiber-reinforced polymer composites: A review. Journal of Industrial Textiles. 2021;50:1165-92.
[21] Liu H, Nie H, Zhang C, Li Y. Loading rate dependency of Mode I interlaminar fracture toughness for unidirectional composite laminates. Composites Science and Technology. 2018;167:215-23.
[22] Isakov M, May M, Hahn P, Paul H, Nishi M. Fracture toughness measurement without force data – Application to high rate DCB on CFRP. Composites Part A: Applied Science and Manufacturing. 2019;119:176-87.
[23] Riezzo MA, Simmons M, Russell B, Sket F, Martínez V, González C. Dynamic characterisation of interlaminar fracture toughness in carbon fibre epoxy composite laminates. Composites Part A: Applied Science and Manufacturing. 2019;126:105597.
[24] Kuhn P, Catalanotti G, Xavier J, Camanho PP, Koerber H. Fracture toughness and crack resistance curves for fiber compressive failure mode in polymer composites under high rate loading. Composite Structures. 2017;182:164-75.
[25] Kuhn P, Catalanotti G, Xavier J, Ploeckl M, Koerber H. Determination of the crack resistance curve for intralaminar fiber tensile failure mode in polymer composites under high rate loading. Composite Structures. 2018;204:276-87.
[26] Catalanotti G, Kuhn P, Xavier J, Koerber H. High strain rate characterisation of intralaminar fracture toughness of GFRPs for longitudinal tension and compression failure. Composite Structures. 2020;240:112068.
[27] Yoo S, Schueler D, Brodbeck M, Toso N, Catalanotti G, Voggenreiter H. An Improved Load Introduction Technique for Dynamic Material Characterisation at Intermediate Strain Rate. Proceedings. 2018;2:381.
[28] Yoo S, Catalanotti G, Toso N, Toso Y, Voggenreiter H. Improvement on dynamic material characterisation of carbon/epoxy composites at intermediate strain rates. In: ICCM22 2019 Melbourne, VIC: Engineers Australia, 2019: 3914-3922: Engineers Australia; 2019.
[29] Yoo S, Dahale M, Neale G, Toso N, Catalanotti G, McIlhagger A, et al. Experimental Investigations of 3D Woven Layer to-Layer Carbon/Epoxy Composites at Different Strain Rates. EPJ Web Conf. 2021;250:01029.
[30] Product Data Sheet HexPly 8852 Epoxy matrix (180°C/356°F curing matrix). Hexcel Corporation 2016.
[31] Koerber H, Kuhn P, Ploeckl M, Otero F, Gerbaud P-W, Rolfes R, et al. Experimental characterization and constitutive modeling of the non-linear stress–strain behavior of unidirectional carbon–epoxy under high strain rate loading. Advanced Modeling and Simulation in Engineering Sciences. 2018;5:17.
[32] Ledford N, Paul H, Ganzenmüller G, May M, Höfemann M, Otto M, et al. Investigations on specimen design and mounting for Split Hopkinson Tension Bar (SHTB) experiments. EPJ Web of Conferences. 2015;94:01049.
[33] Ploeckl M, Kuhn P, Grosser J, Wolfahrt M, Koerber H. A dynamic test methodology for analyzing the strain-rate effect on the longitudinal compressive behavior of fiber-reinforced composites. Composite Structures. 2017;180:429-38.
[34] ASTM D3039 / D3039M-17, Standard Test Method for Tensile Properties of Polymer Matrix Composite Materials. West Conshohocken, PA, : ASTM International; 2017.

[35] ASTM D3518 / D3518M-18, Standard Test Method for In-Plane Shear Response of Polymer Matrix Composite Materials by Tensile Test of a ±45° Laminate. West Conshohocken, PA: ASTM International; 2018.
[36] Rusinek A, Jankowiak T. Dynamic Behavior of Materials. Constitutive Relations and Applications. In: Łodygowski T, Rusinek A, editors. Constitutive Relations under Impact Loadings: Experiments, Theoretical and Numerical Aspects. Vienna: Springer Vienna; 2014. p. 87-135.
[37] Briers WJ. Overcoming Challenges in Material Characterization of Polymers at Intermediate Strain Rates. Cham: Springer International Publishing; 2015. p. 153-64.
[38] Uriarte I, Garitaonandia I, Guraya T, Arriaga A. Suppression of ringing oscillations from high speed rubber compression curves through a detailed modal characterization of servo-hydraulic machines. Polymer Testing. 2017;60:365-73.
[39] Catalanotti G, Arteiro A, Hayati M, Camanho PP. Determination of the mode I crack resistance curve of polymer composites using the size-effect law. Engineering Fracture Mechanics. 2014;118:49-65.
[40] Harding J, Welsh LM. A tensile testing technique for fibre-reinforced composites at impact rates of strain. Journal of Materials Science. 1983;18:1810-26.
[41] Taniguchi N, Nishiwaki T, Kawada H. Tensile strength of unidirectional CFRP laminate under high strain rate. Advanced Composite Materials. 2007;16:167-80.
[42] Herakovich CT, Schroedter RD, Gasser A, Guitard L. Damage evolution in [±45]s laminates with fiber rotation. Composites Science and Technology. 2000;60:2781-9.
[43] R. Wisnom M. The effect of fibre rotation in ±45° tension tests on measured shear properties. Composites. 1995;26:25-32.
[44] Cui H, Thomson D, Pellegrino A, Wiegand J, Petrinic N. Effect of strain rate and fibre rotation on the in-plane shear response of ±45° laminates in tension and compression tests. Composites Science and Technology. 2016;135:106-15.
[45] Gilat A, Goldberg RK, Roberts GD. Experimental study of strain-rate-dependent behavior of carbon/epoxy composite. Composites Science and Technology. 2002;62:1469-76.
[46] Kwon J, Choi J, Huh H, Lee J. Evaluation of the effect of the strain rate on the tensile properties of carbon–epoxy composite laminates. Journal of Composite Materials. 2017;51:3197-210.
[47] Lienhard J, Böhme W. Characterisation of resin transfer moulded composite laminates under high rate tension, compression and shear loading. Engineering Fracture Mechanics. 2015;149:338-50.
[48] Hsiao HM, Daniel IM, Cordes RD. Strain Rate Effects on the Transverse Compressive and Shear Behavior of Unidirectional Composites. Journal of Composite Materials. 1999;33:1620-42.
[49] Schaefer JD, Werner BT, Daniel IM. Strain-Rate-Dependent Failure of a Toughened Matrix Composite. Experimental Mechanics. 2014;54:1111-20.
[50] Koerber H, Xavier J, Camanho PP. High strain rate characterisation of unidirectional carbon-epoxy IM7-8552 in transverse compression and in-plane shear using digital image correlation. Mechanics of Materials. 2010;42:1004-19.
[51] Tsai J-L, Sun CT. Strain rate effect on in-plane shear strength of unidirectional polymeric composites. Composites Science and Technology. 2005;65:1941-7.
[52] Daniel IM, Daniel SM, Fenner JS. A new yield and failure theory for composite materials under static and dynamic loading. International Journal of Solids and Structures. 2018;148-149:79-93.
[53] Gowtham HL, Pothnis JR, Ravikumar G, Naik NK. High strain rate in-plane shear behavior of composites. Polymer Testing. 2013;32:1334-41.
[54] Shokrieh MM, Omidi MJ. Investigation of strain rate effects on in-plane shear properties of glass/epoxy composites. Composite Structures. 2009;91:95-102.
[55] Taniguchi N, Nishiwaki T, Kawada H. Experimental Characterization of Dynamic Tensile Strength in Unidirectional Carbon/Epoxy Composites. Advanced Composite Materials. 2008;17:139-56.
[56] Staab GH, Gilat A. High Strain Rate Response of Angle-Ply Glass/Epoxy Laminates. Journal of Composite Materials. 1995;29:1308-20.
[57] Camanho PP, Maimí P, Dávila CG. Prediction of size effects in notched laminates using continuum damage mechanics. Composites Science and Technology. 2007;67:2715-27.
[58] Catalanotti G, Camanho PP, Xavier J, Dávila CG, Marques AT. Measurement of resistance curves in the longitudinal failure of composites using digital image correlation. Composites Science and Technology. 2010;70:1986-93.

[59] Hoffmann J, Cui H, Petrinic N. Determination of the strain-energy release rate of a composite laminate under high-rate tensile deformation in fibre direction. Composites Science and Technology. 2018;164:110-9.
[60] Laffan MJ, Pinho ST, Robinson P, McMillan AJ. Translaminar fracture toughness: The critical notch tip radius of 0° plies in CFRP. Composites Science and Technology. 2011;72:97-102.
[61] Li X, Hallett SR, Wisnom MR, Zobeiry N, Vaziri R, Poursartip A. Experimental study of damage propagation in Over-height Compact Tension tests. Composites Part A: Applied Science and Manufacturing. 2009;40:1891-9.
[62] McCarroll CA. High rate fracture toughness measurement of laminated composites. South Kensington, London: Imperial College London, 2011.
[63] Xu X, Wisnom MR, Mahadik Y, Hallett SR. Scaling of fracture response in Over-height Compact Tension tests. Composites Part A: Applied Science and Manufacturing. 2015;69:40-8.
[64] Czabaj MW, Ratcliffe JG. Comparison of intralaminar and interlaminar mode I fracture toughnesses of a unidirectional IM7/8552 carbon/epoxy composite. Composites Science and Technology. 2013;89:15-23.

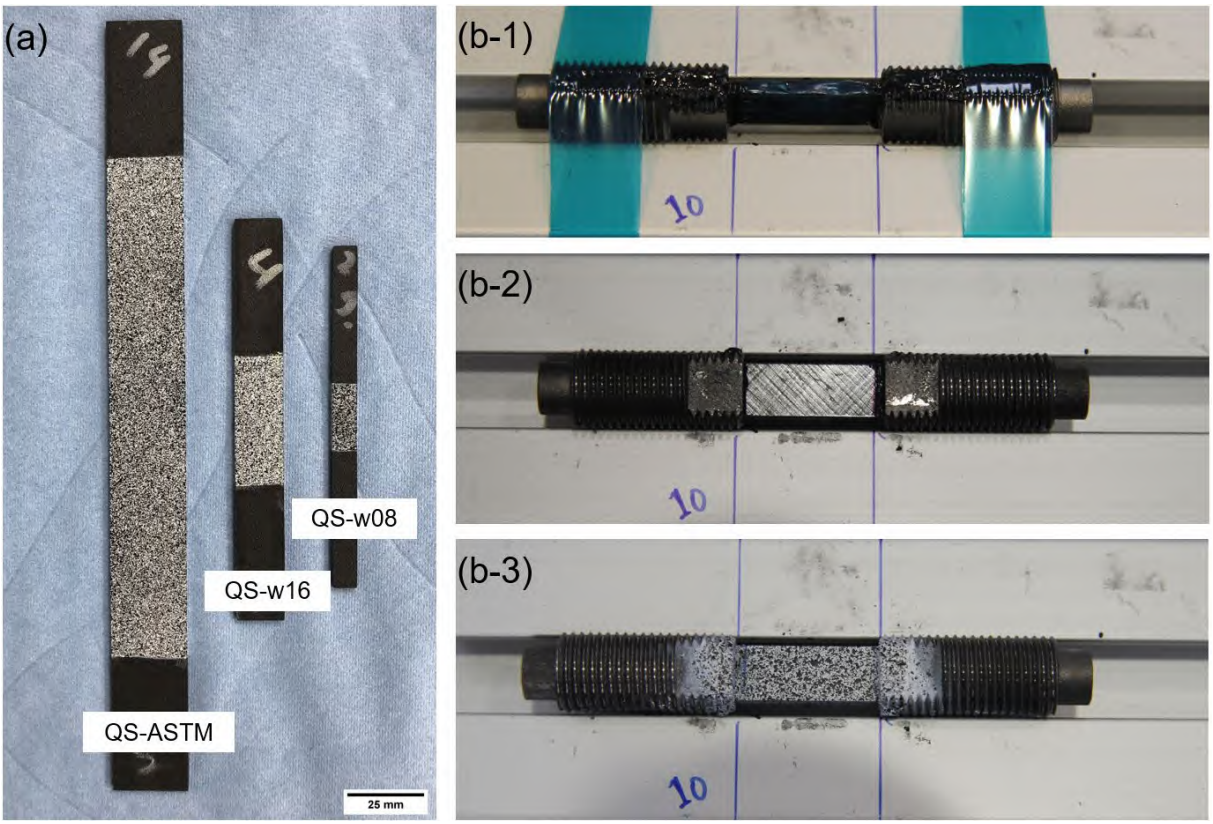

Figure 1: Images of ± 45° tensile specimens for in-plane shear testing; (a) for the quasi-static, and (b) sample preparation steps for dynamic testing at intermediate strain rates using adhesive clamping technique.

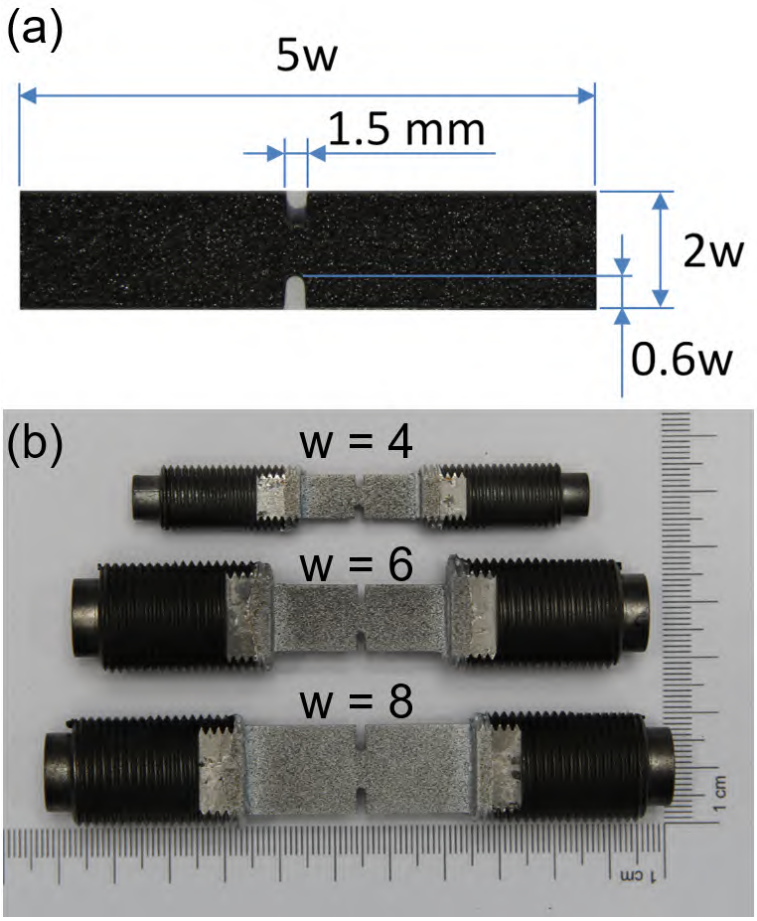

Figure 2: Images of Double-edge notched tension (DENT) specimens; (a) Geometry for the gauge section of the intralaminar fracture toughness DENT specimens; (b) three sizes of speckled DENT specimens in the threaded grips for intermediate strain rate testing.

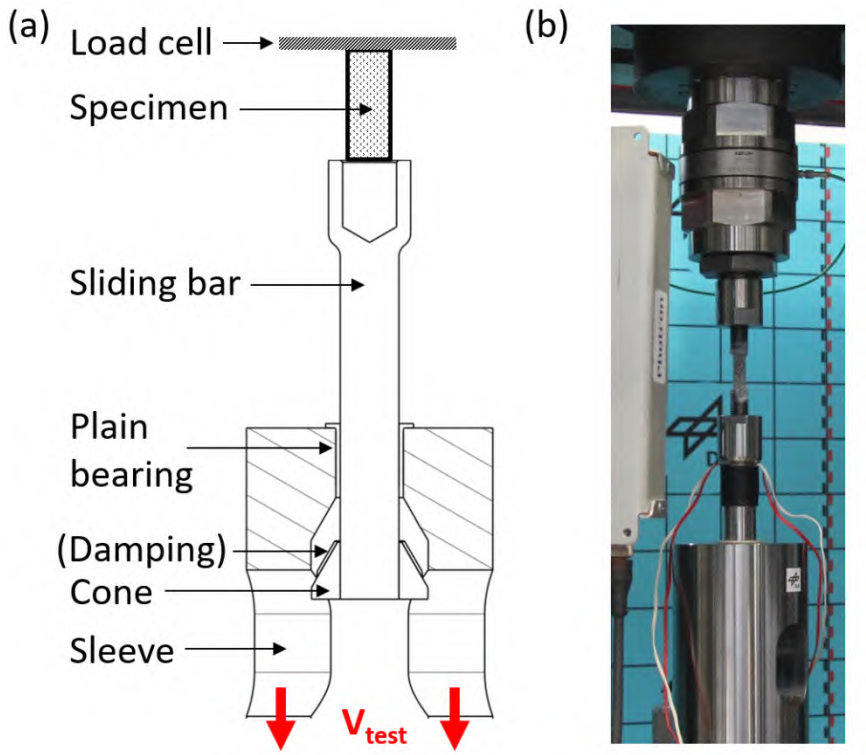

Figure 3. The developed slack adapter: (a) Cross-sectional representation; (b) placed within the high-speed servo-hydraulic machine set-up.

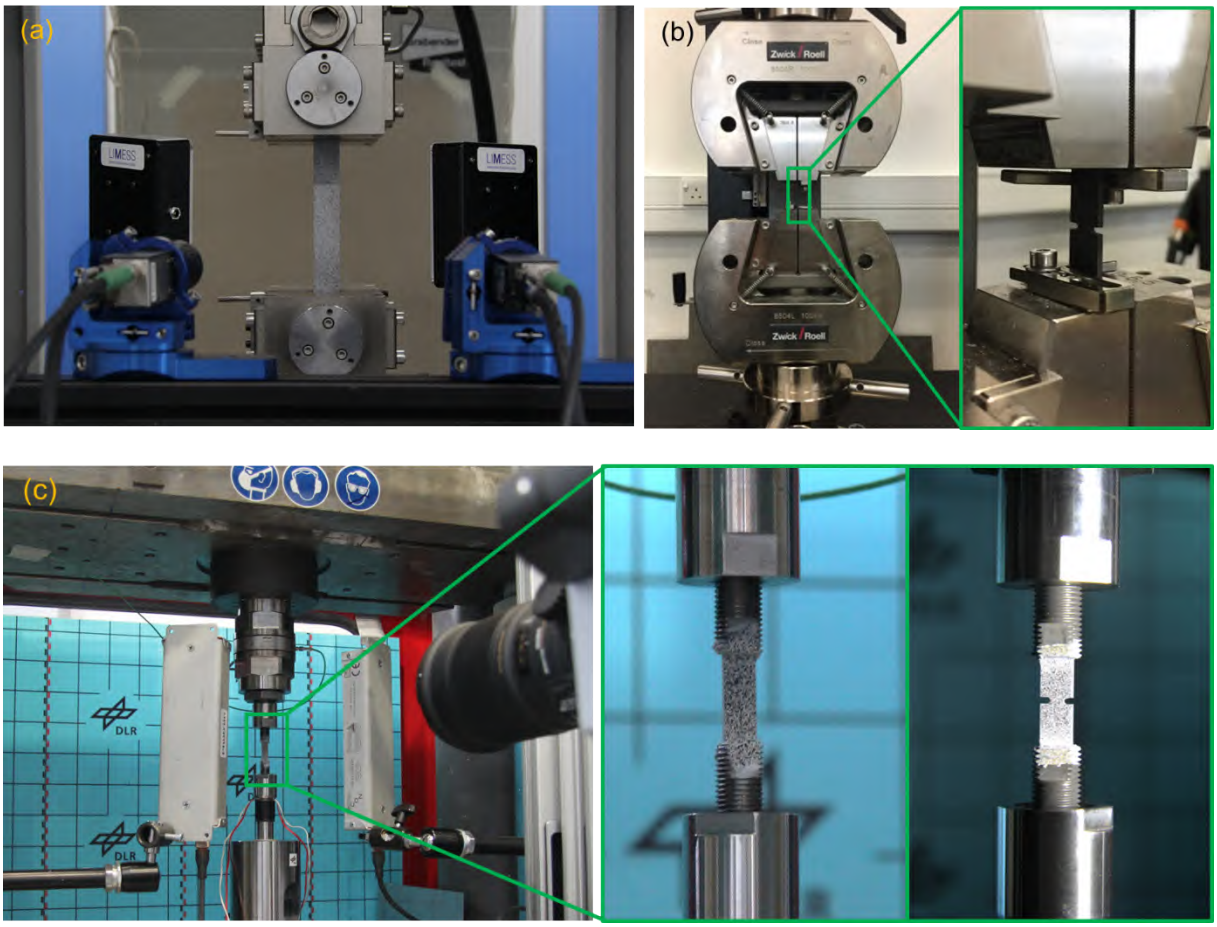

Figure 4. Test set-ups for; (a) quasi-static testing of ± 45° tensile specimens, (b) quasi-static testing of DENT specimens, and (c) intermediate strain rate testing of both specimen types and a zoom up image: in-plane shear (left) and DENT (right) specimens.

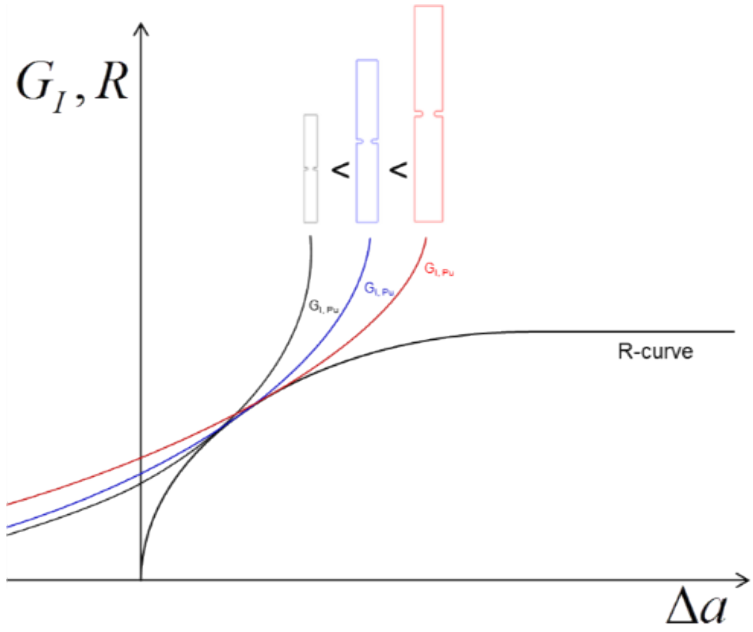

Figure 5: *R*-curve as an envelope of peak load driving force curves for geometrically scaled specimens.

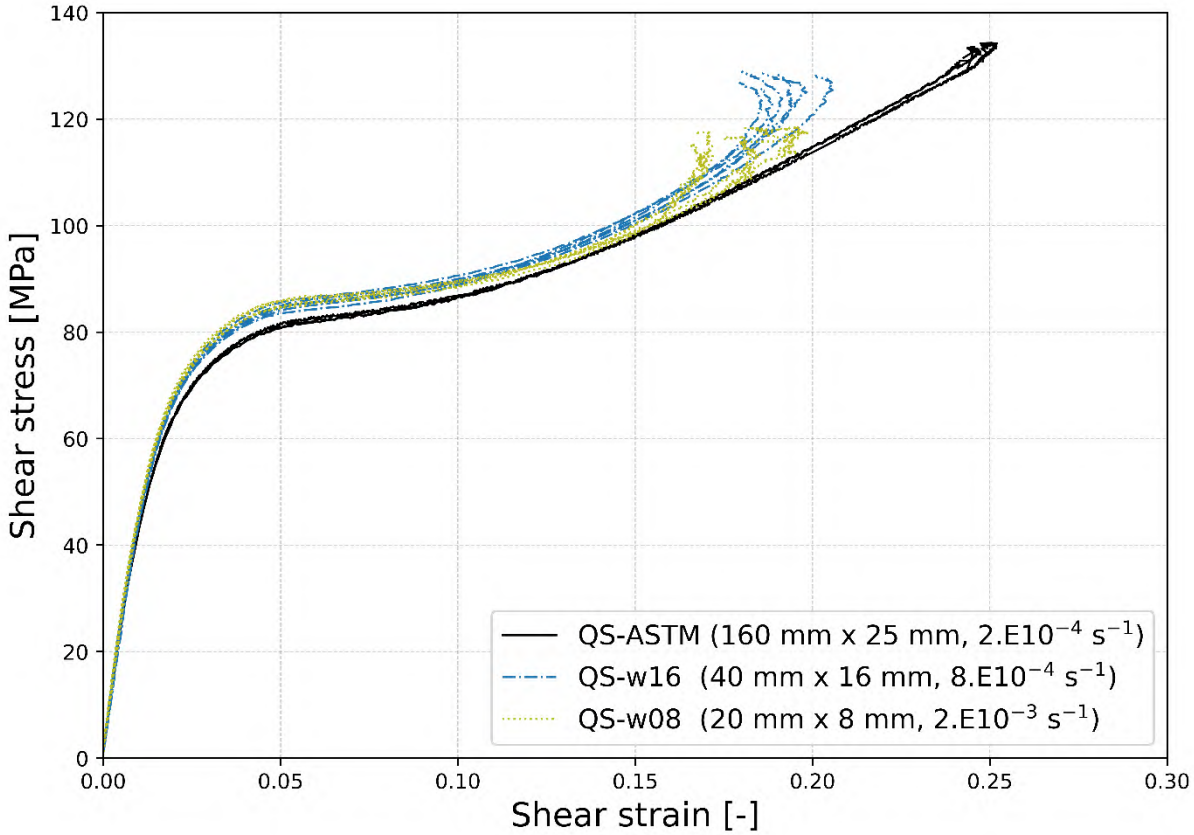

Figure 6: Quasi-static in-plane shear stress-strain data for three different ± 45° tensile specimen geometries.

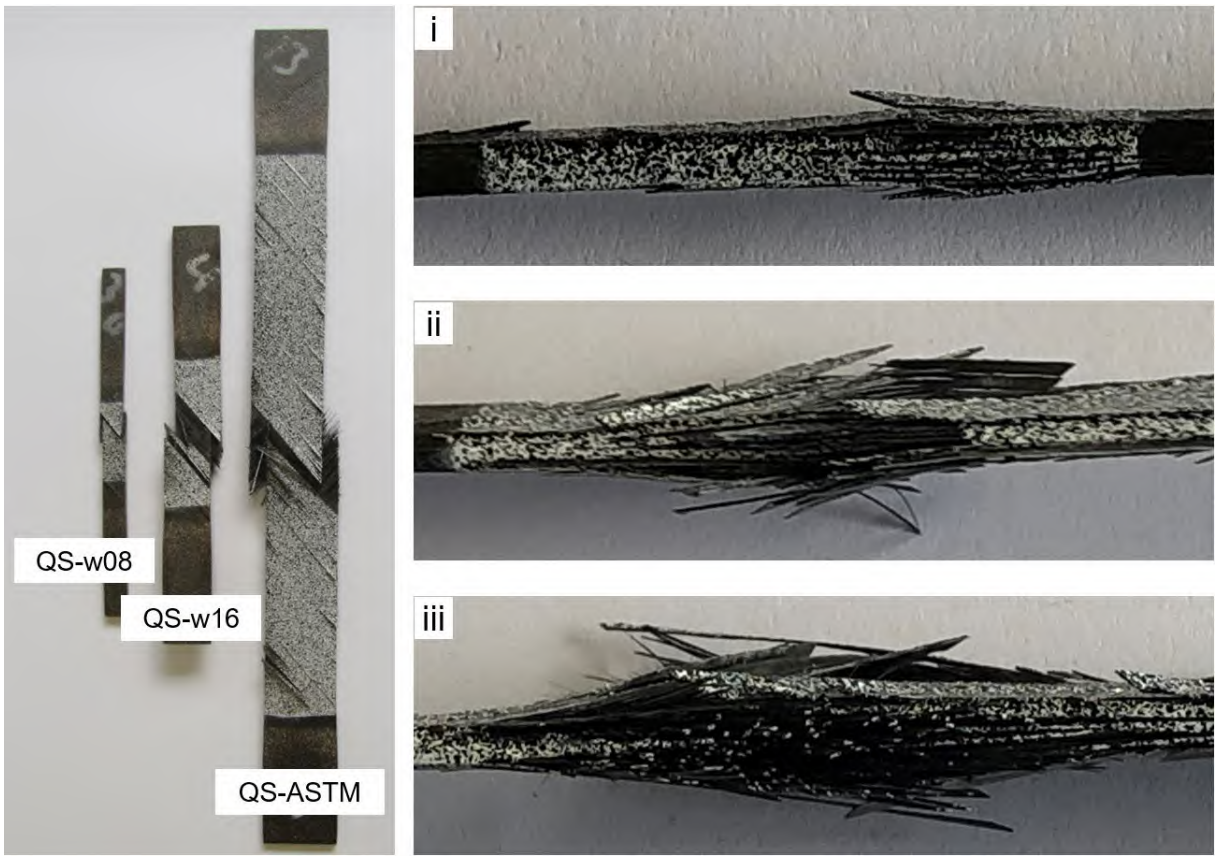

Figure 7: Images of the quasi-statically tested ± 45° tensile specimens front (left) and side (right) views of different specimen geometries (i – QS-w08, ii – QS-w16, and iii – QS-ASTM).

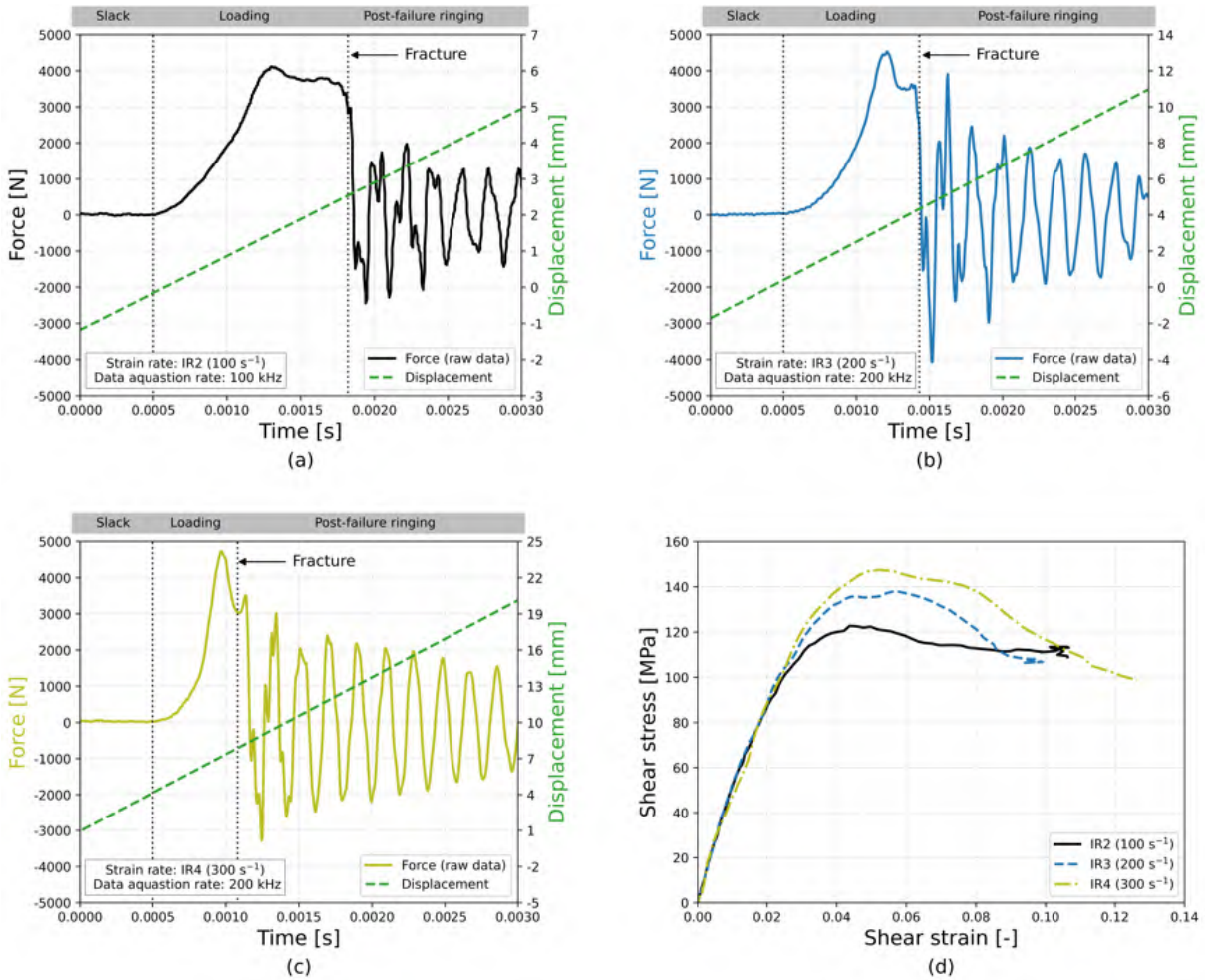

Figure 8: Comparison of raw force-time signals, including displacement profiles, from dynamic in-plane shear testing at different nominal strain rates: (a) 100 s^{-1}; (b) 200 s^{-1}; (c) 300 s^{-1}; and (d) their derived dynamic shear stress-strain data.

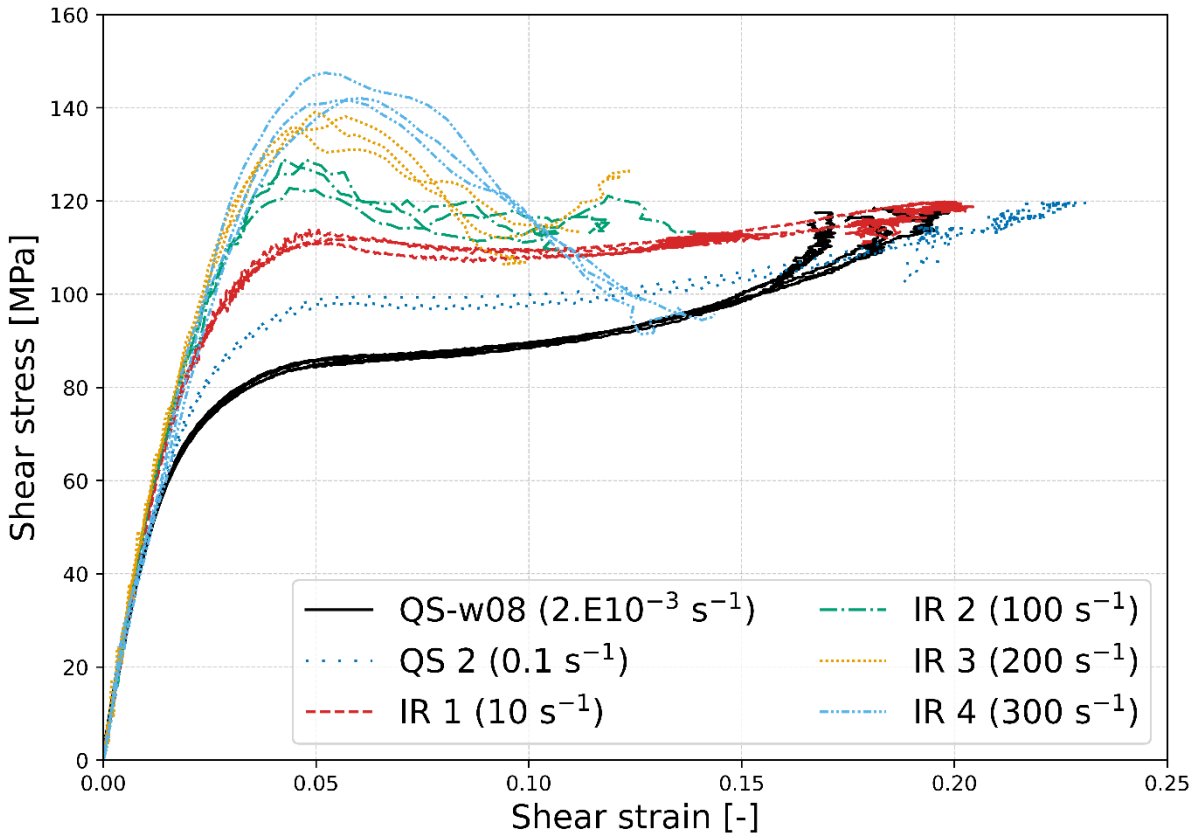

Figure 9: Comparison of quasi-static and dynamic in-plane shear stress-strain data obtained from ± 45° tensile specimens.

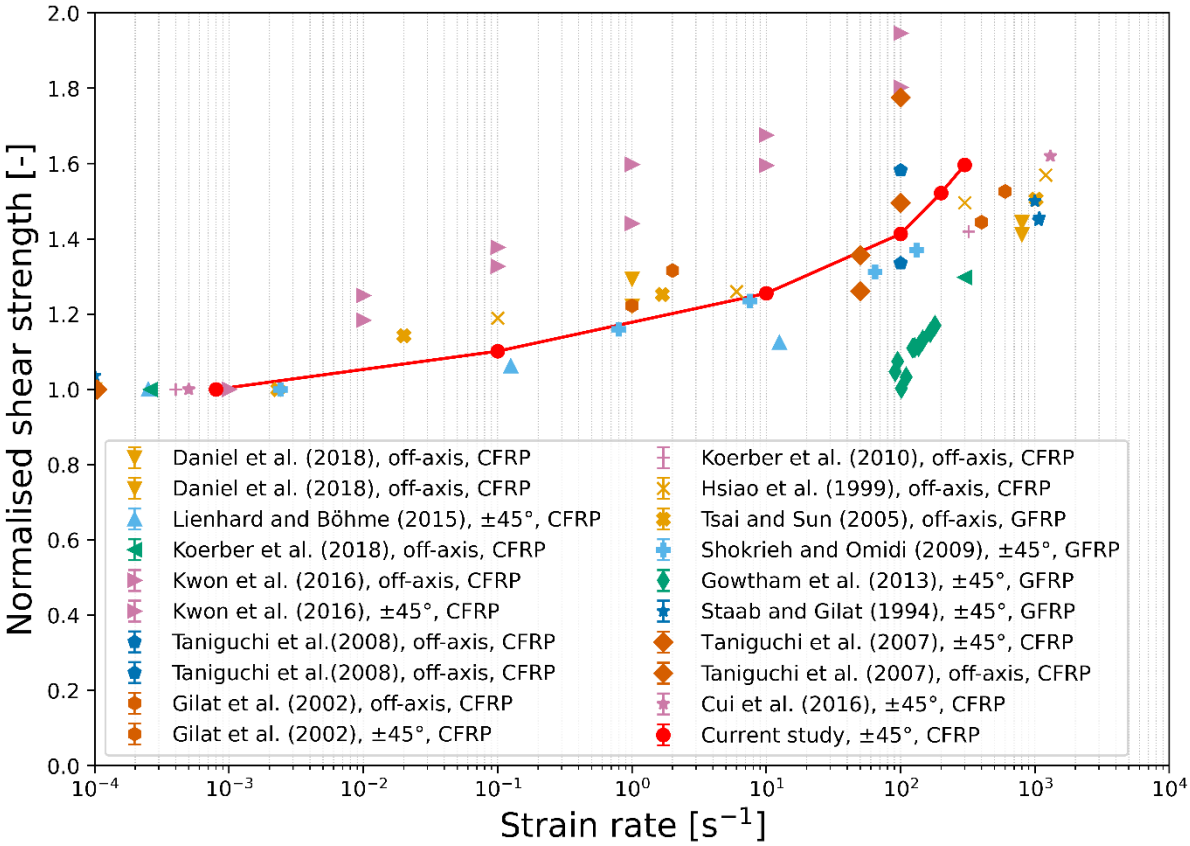

Figure 10: Comparison of published experimental results on in-plane shear strength [31, 41, 44-48, 50-56] with the values obtained from the current study.

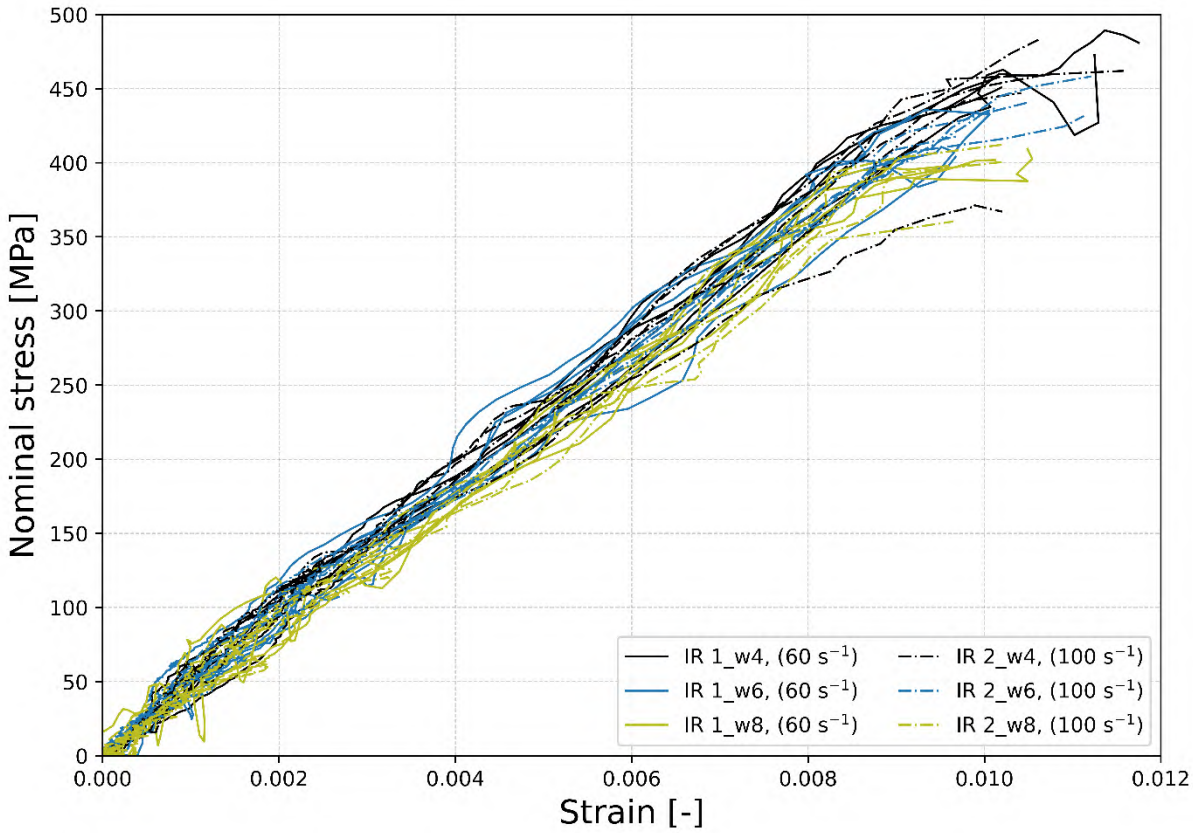

Figure 11: Dynamic nominal stress-strain data of IM7/8552 DENT specimens tested at strain rates of 60 s^{-1} and 100 s^{-1}.

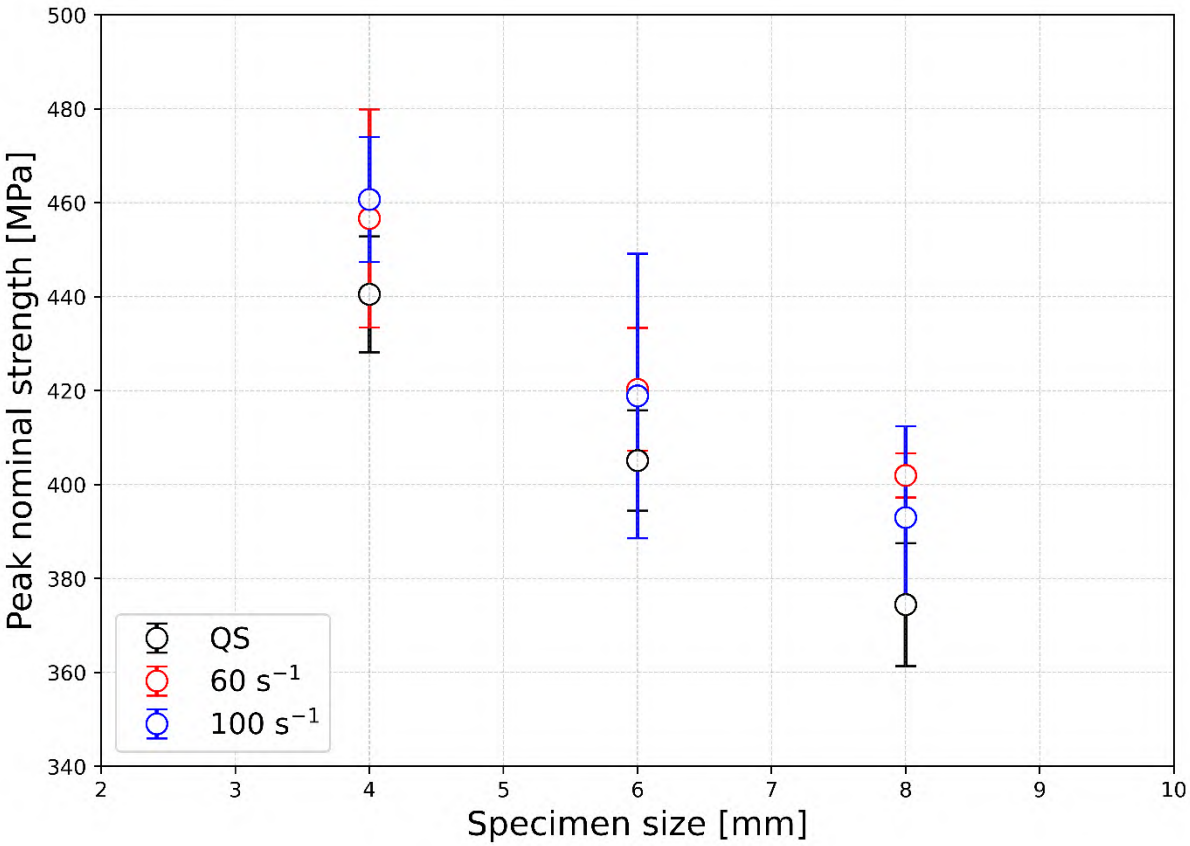

Figure 12: Peak nominal stress (σ_u) variation with characteristic specimen size (w) measured at different loading rates from the quasi-static (QS) up to strain rate of 100 s^{-1}.

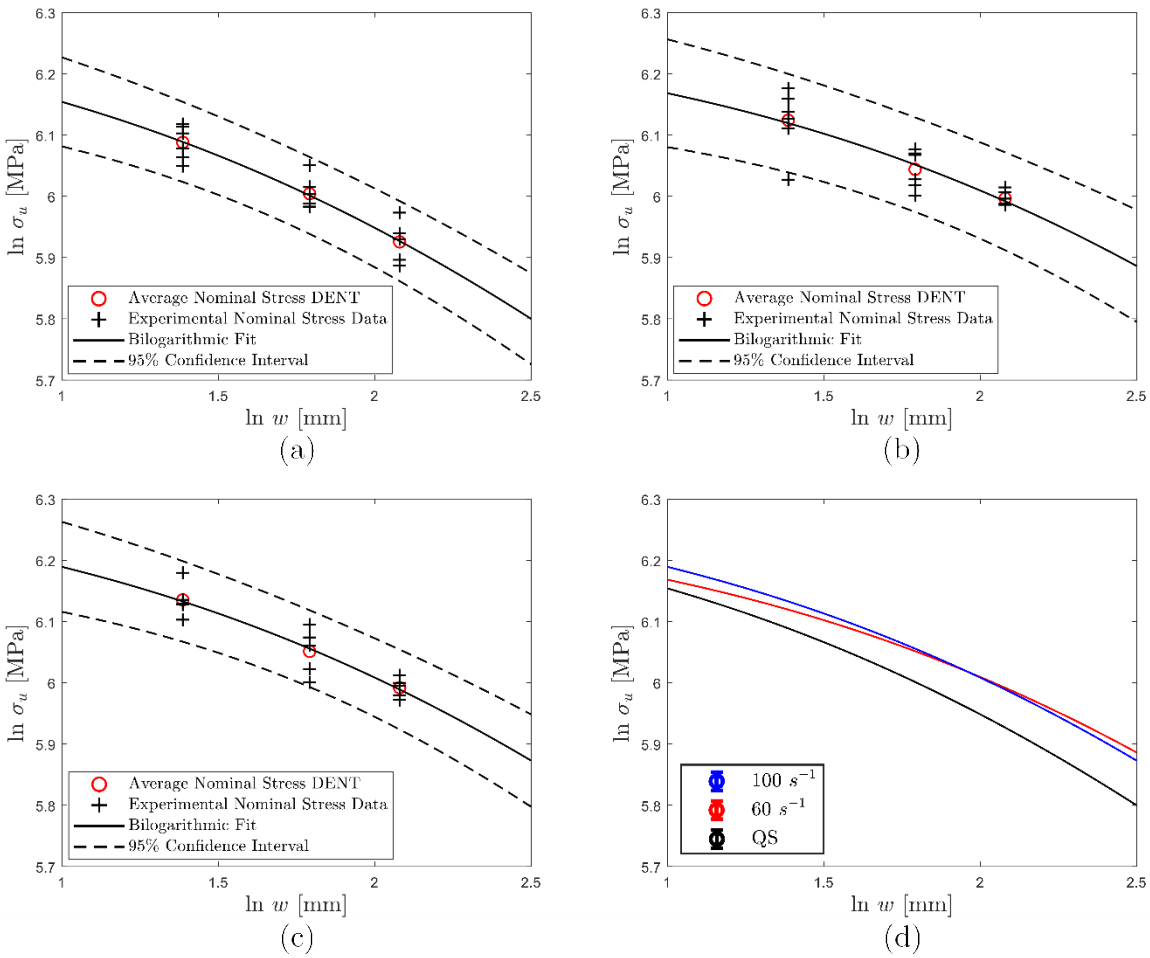

Figure 13: Bilogarithmic size effect fittings: (a) quasi-static (QS); (b) 60 s^{-1} (IR 1); (c) 100 s^{-1} (IR 2); and (d) a comparison.

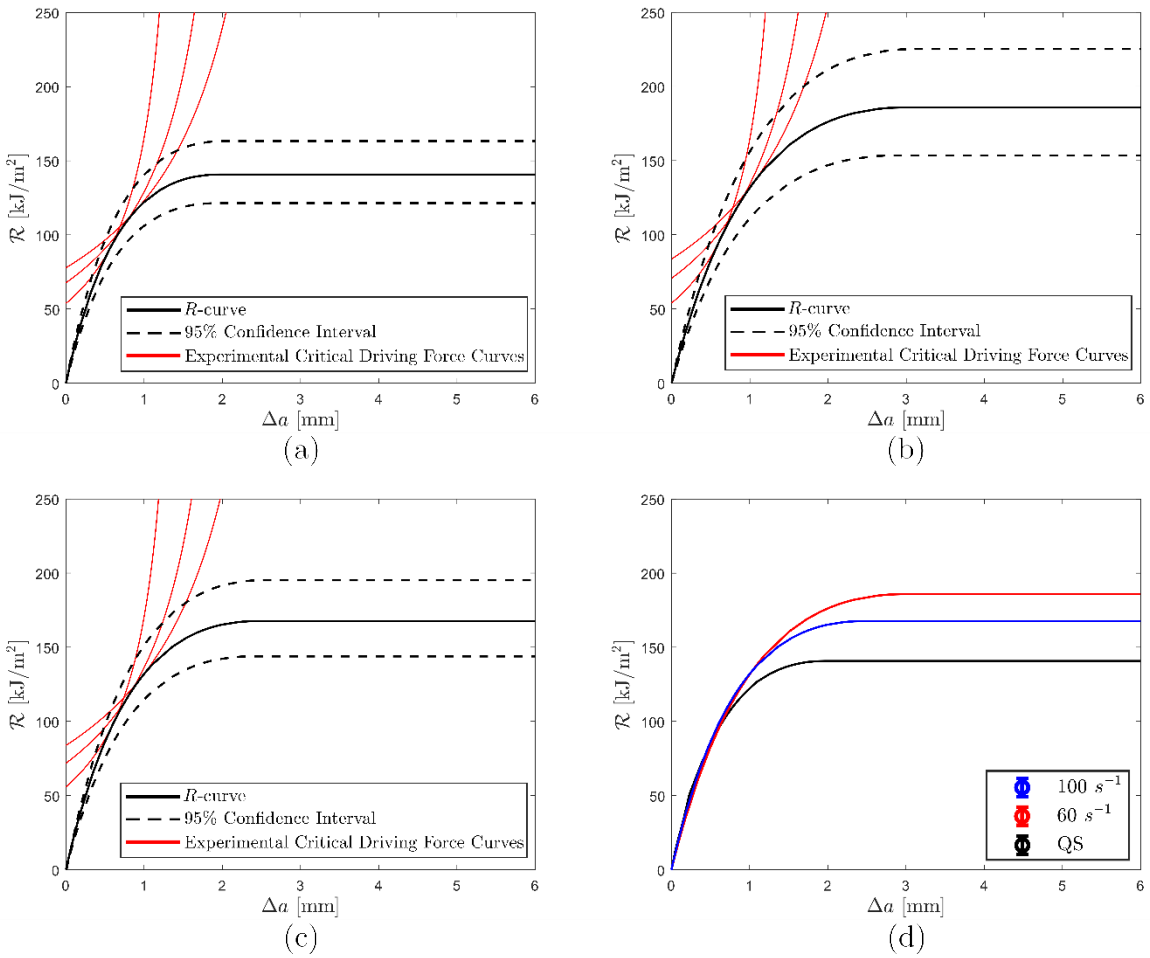

Figure 14: Size-independent mode I intralaminar *R*-curves: (a) quasi-static (QS); (b) 60 s^{-1} (IR 1); (c) 100 s^{-1} (IR 2); and (d) a comparison.

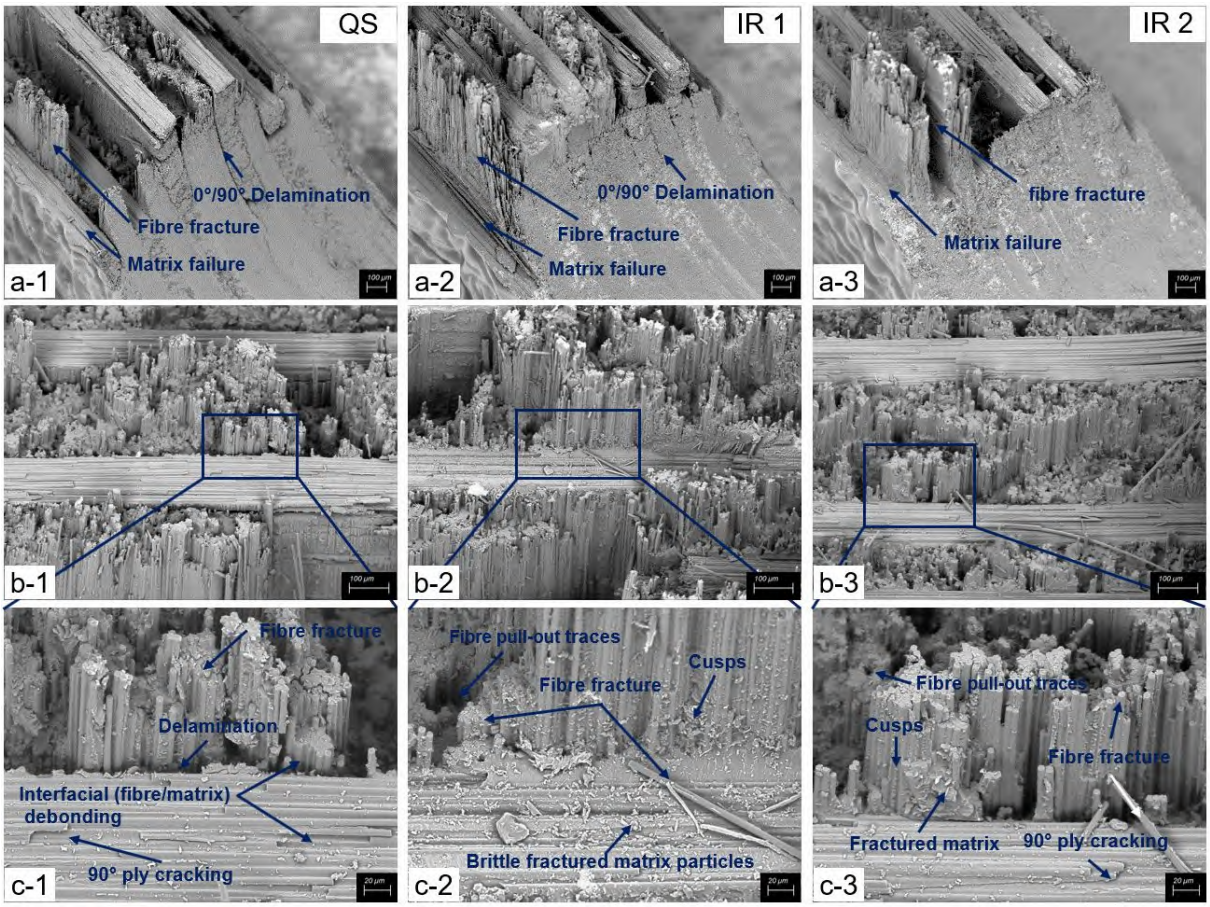

Figure 15: SEM fractography of DENT specimens tested at various strain rates: 1. quasi-static (QS), 2. 60 s^{-1} (IR 1), and 3. 100 s^{-1} (IR 2). Image locations: (a) at the initial notch tip; (b) at a 0°/90° fracture surface interface; and (c) a magnification of (b).

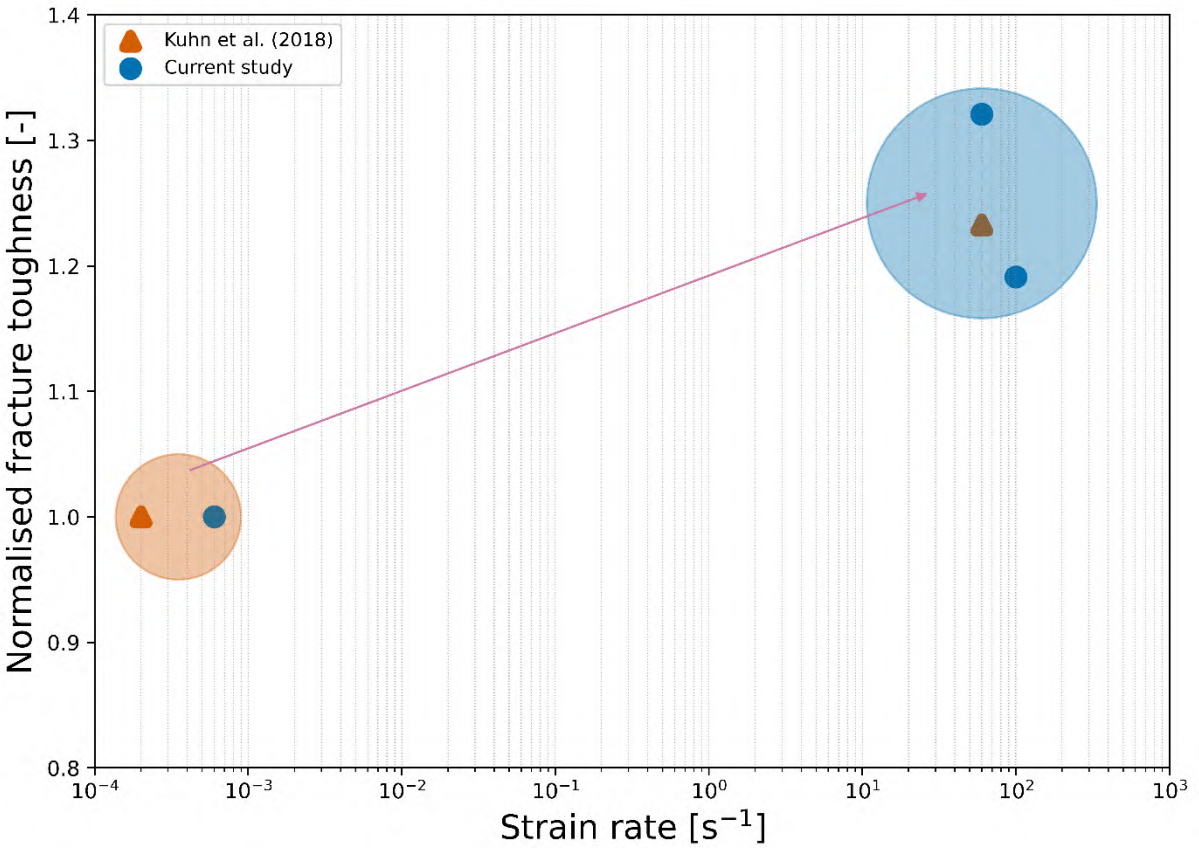

Figure 16: Comparison of the normalised steady-state mode I intralaminar fracture toughness of IM7/8552 measured at different loading rates from quasi-static to strain rates up to 100 s^{-1}.

Table 1: Summary of the quasi-static specimen geometries for in-plane shear testing.

Specimen Type	Gauge section size [mm]		Length-to-width ratio	Number of tested specimens
	Length	Width		
QS_ASTM	160	25	6.4	3
QS_w16	40	16	2.5	6
QS_w08	20	8	2.5	6

Table 2: Summary of dynamic in-plane shear properties of IM7/8552 carbon-epoxy composite, and corresponding parameters for digital image correlation (DIC).

Strain rate [s^{-1}]	G_{xy} [GPa]	τ_{xy} at 5 % strain [MPa]	τ_{xy} at 0.2 % offset [MPa]	Resolution [pixels]	Frame rates [fps]
QS_ASTM	4.68 ± 0.23	81.09 ± 0.48	49.09 ± 1.88	4096 × 1215	2
QS_w16	4.71 ± 0.10	86.32 ± 0.88	54.98 ± 1.90	4096 × 3000	1
QS_w08	4.52 ± 0.37	88.84 ± 0.67	54.06 ± 3.26	4096 × 3000	0.5
0.1 (QS 2)	4.82 ± 0.25	97.85 ± 0.91	59.66 ± 2.16	512 × 176	250
10 (IR 1)	5.47 ± 0.15	111.52 ± 0.98	66.31 ± 0.67	512 × 176	50k
100 (IR 2)	5.35 ± 0.22	125.54 ± 2.92	75.15 ± 1.26	512 × 176	100k
200 (IR 3)	5.78 ± 0.13	135.20 ± 3.63	71.06 ± 3.91	384 × 176	200k
300 (IR 4)	5.50 ± 0.29	141.81 ± 4.98	69.42 ± 5.68	384 × 176	200k

Table 3: IM7/8552 cross-ply laminate elastic properties used in the VCCT models.

Strain rate [s^{-1}]	E [GPa]	G_{xy} [GPa]	ν_{xy} [-]	ρ [-]	λ [-]	$\acute{E}$ [GPa]
0.0006 (QS)	85.31 ± 2.99 (C.V. = 3.5 %)	4.52 ± 0.37 (C.V. = 8.3 %)	0.029 ± 0.003 (C.V. = 10.0 %)	9.08	1	37.99
60 (IR 1)	85.31 ± 2.99* (= QS)	5.47 ± 0.15** (C.V. = 2.8 %)	0.051 ± 0.004*** (C.V.= 8.1 %)	7.74	1	40.81
100 (IR 2)	85.31 ± 2.99* (= QS)	5.35 ± 0.22 (C.V. = 4.0 %)	0.051 ± 0.006*** (C.V. = 11.0 %)	7.92	1	40.39

* assumed no strain rate dependency.
** taken from the results measured at a strain rate of 10 s^{-1}.
*** estimated using DIC strains from the linear portions of the DENT specimens (w=4) at low load.

Table 4: Average peak nominal stress of double-edge notched tension (DENT) specimens measured at quasi-static and intermediate strain rates.

Strain rate [s^{-1}]	$w = 4$	$w = 6$	$w = 8$
0.0006 (QS)	440.52 ± 12.35 (C.V. = 2.8 %)	405.13 ± 10.70 (C.V. = 2.6 %)	374.46 ± 13.08 (C.V. = 3.5 %)
60 (IR 1)	456.68 ± 23.23 (C.V. = 5.1 %)	420.28 ± 13.07 (C.V. = 3.1 %)	401.97 ± 4.72 (C.V. = 1.2 %)
100 (IR 2)	460.72 ± 13.32 (C.V. = 2.9 %)	418.88 ± 30.29 (C.V. = 7.2 %)	393.00 ± 19.46 (C.V. = 5.0 %)

Table 5: Summary of the steady-state fracture toughness, critical crack extension, and fitting coefficients of the bilogarithmic size effect law, for the cross-ply specimens tested at varying strain rates.

Strain rate [s^{-1}]	R_{SS} [kJ/m^2]	c_f [mm]	M [$MPa\sqrt{mm}$]	N [mm]
0.0006 (QS)	140.7	2.0	1426.0	6.5
60 (IR 1)	185.9	3.0	1686.8	9.8
100 (IR 2)	167.6	2.4	1596.1	8.0

Table 6: Comparison of the quasi-static mode I intralaminar fracture toughness (G_{Ic}) of UD IM7/8552 composites reported in the literature, for the 0^0 ply.

Name	Lay-up	Test method	G_{IC} [kJ/m^2]	SD	CV
Current work	$[90/0]_{3s}$	DENT	281.5 (G_{Ic}* = 140.7)		
Catalanotti et al. (2014) [39]	$[90/0]_{4s}$	DENT	205		
Kuhn et al. (2018) [25]	$[90/0]_{3s}$	DENT	195.5		
Camanho et al. (2007) [57]	$[90/0]_{8s}$	CT	81.5	6.1	7.6
Hoffamnn (2018) [59]	$[(90/0)_8/90]_s$	CT	195.8	18	
Catalanotti et al. (2010) [58]	$[90/0]_{8s}$	CT	133.7		
McCarroll (2011)* [62]	$[(90/0)_8/90]_s$	CT	74.9		9.1
Laffan et al. (2011) [60]	$[(90/0)_8/90]_s$	CT	147.2	12.1	8.2
Xu et al. (2015)* [63]	$[45/90/-45/0]_{4s}$	OCT	67.1		2.8
Li et al. (2009)* [61]	$[0/90]_{4s}$	OCT	149.9		
Li et al. (2009)* [61]	$[0/90]_{8s}$	OCT	145.9		

* G_{Ic} of the laminate (equal to half the G_{Ic} of the 0^0 ply).

Declaration of interests

☒ The authors declare that they have no known competing financial interests or personal relationships that could have appeared to influence the work reported in this paper.

☐ The authors declare the following financial interests/personal relationships which may be considered as potential competing interests:

CRediT authorship contribution statement

Sanghyun Yoo: Conceptualisation, Methodology, Investigation, Validation, Writing-Original draft preparation, Data Curation, Visualisation, Formal analysis. **Denis Dalli:** Methodology, Visualisation, Formal analysis, Writing-Review & Editing. **Giuseppe Catalanotti:** Conceptualisation, Methodology, Writing-Review & Editing. **Nathalie Toso:** Conceptualisation, Resources, Methodology, Writing-Review & Editing, Supervision, Funding acquisition, Project administration. **Fiona Kessel:** Methodology, Data Curation. **Heinz Voggenreiter:** Supervision, Funding acquisition.